Chapter 10

CMS HIGH-GRANULARITY CALORIMETER TIMING LAYER

10.1 Introduction

Recent advances in silicon sensors in terms of radiation tolerance, highly granular desings [16], and cost per unit area offers the possibility of their use as the sentive media in a sampling calorimeter at the HL-LHC. An important example of such a device is the forward calorimeter proposed for the CMS Phase 2 Upgrade [45], where high-granularity silicon sensors and tungsten/copper absorber layers are interleaved. As described in Chapter 9, silicon-based shower maximum detectors have extremely good precision timing capabilities – achieving a TOF resolution of 25 ps for 32 GeV electron induced shower – which could be use to reduce the detrimental effects of the high pileup enviroment foreseen for the HL-LHC. This chapter presents recents studies on the intrinsic timing properties of the silicon sensors to be used by the proposed CMS high-granularity calorimeter (HGC).

This chapter is organized as follows. General properties of the HGC silicon sensor are described in Section 10.2. The test beam setup and experimental apparatus are presented in Section 10.3. The results of the test beam measurements are presented in Section 10.4. Finally, Section 10.5 is devoted to discussion and conclusions.

10.2 General Properties of Silicon Timing and Bench Test Studies

All measurements presented in this chapter were carried out using a silicon sensor identical to that of the CMS HGC. The silicon sensor thickness is 300μm and it is comprised of 128 hexagonal pixels with 1 cm maximal diameter. The left and right panels of Figure 10.1 show an schematic with 7 pixels and a full CAD schematic of the sensor, respectively. The silicon sensor was wire-bonded to a printed circuit board (PCB) where 25 pixels were implemented with an independent analog readout. The PCB provided amplification for all the 25 implemented pixels and was optimized for timing measurement, this final HGC timing layer is shown in Figure 10.2. The silicon sensor was operated with a bias voltage of -300 V and the measured total current was 170 μA.

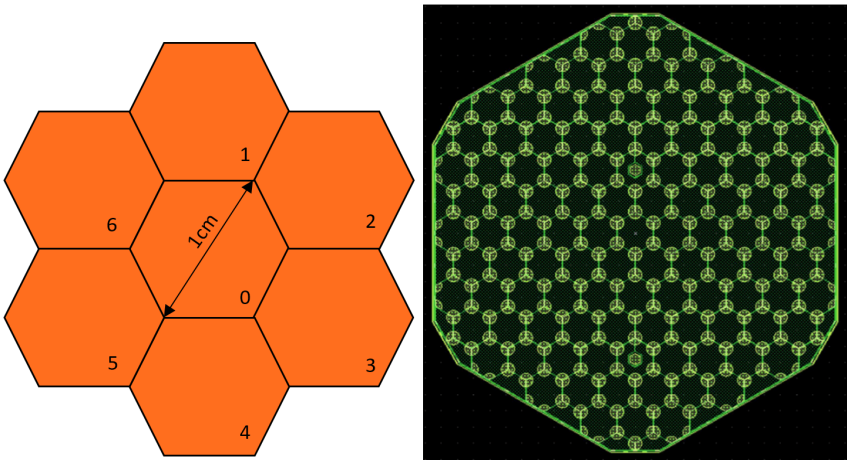

Figure 10.1: An HGC sensor schematic geometry with 7 pixels (left), and a s CAD schematic of the entire sensor (right) are shown.

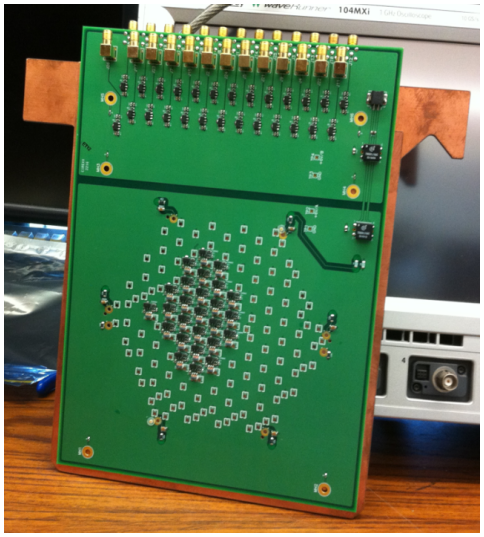

Figure 10.2: The implemented HGC timing layer is shown. 25 pixels with full analog electronics were implemented. The silicon sensor is at the back of the PCB.

10.3 Test-beam Setup and Experimental Apparatus

Test-beam measurements were carried out at the FTBF which provided a 120 GeV proton beam from the Fermilab Main Injector accelerator , and secondary beams composed of electrons, pions, and muons of energies ranging from 4 GeV to 32 GeV. A simple schematic diagram of the experimental setup is shown in Figure 10.3. A small plastic scintillator of transverse dimensions 1.7 mm×2 mm is used as a trigger counter to initiate the read out of the DAQ system and to select incident beam particles from a small geometric area, allowing us to center the beam particles on the

HGC timing layer. Next, we place a stack of either tungsten or lead absorbers of various thicknesses for measurements of the longitudinal profile of the electromagnetic shower. The HGC timing layer is located immediately downstream of the absorber plates. Finally, a Photek 240 MCP-PMT detector [28, 116, 119, 117] is placed furthest downstream, and serves to provide a very precise reference timestamp; Its precision has been previously measured to be less than 10 ps [119]. A photograph showing the various detector components is presented in Figure 10.4. More details of the experimental setup are described in our previous studies using the same experimental facility in references [28, 116, 119, 117] as well as in Chapters 7 and 8. The DAQ system is based on a CAEN V1742 digitizer board [5], which

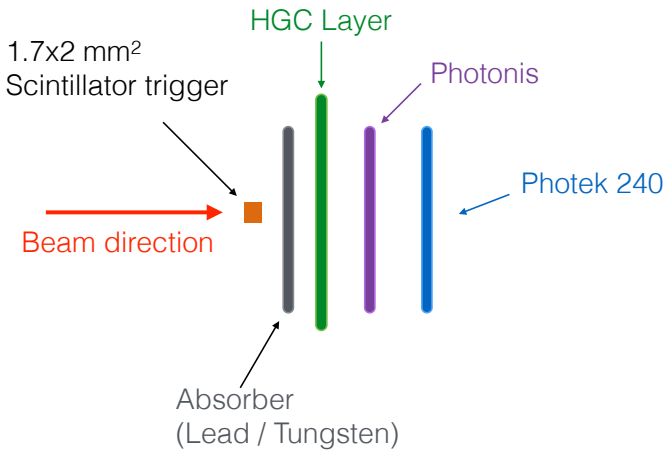

Figure 10.3: A schematic diagram of the test-beam setup is shown. The t_0 and t_1 are defined in Section 9.4.

provides digitized waveforms sampled at 5 GS/s. The HGC timing layer was not electromagneticly shielded and therefore some electronic pickup noise was detected and accounted for during the offline analysis. A nominal bias voltage of -300 V was applied to deplete the silicon sensor in all of the studies shown below.

10.4 Test Beam Measurement, Data Analysis, and Results

Measurements were performed in June 2016, using the primary 120 GeV proton beam, and secondary electron beam provided for the FTBF. Secondary beams with energies ranging from 4 GeV to 32 GeV were used. As discussed in Chapter 9, the electron purity for those beams ranges between 70% at the lowest energy to about 10% at the highest energy. Stacks of either tungsten or lead plates with varying thicknesses were placed immediately upstream of the HGC timing layer in order to measure the response along the longitudinal direction of the electromagnetic

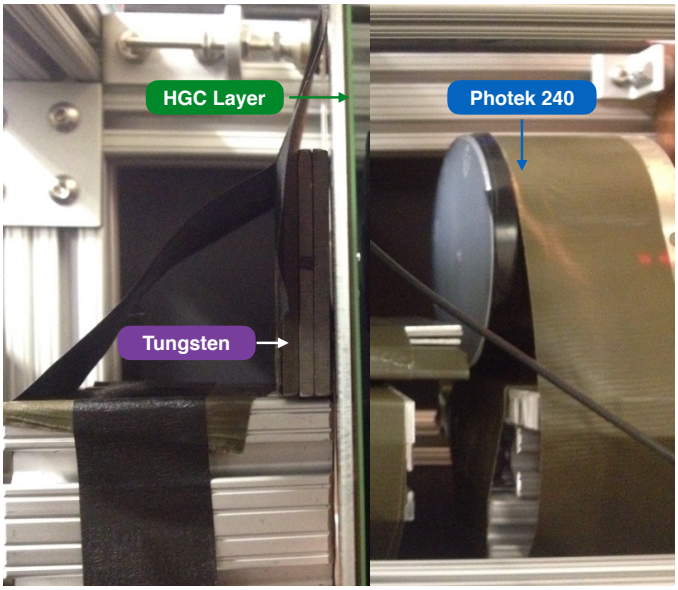

Figure 10.4: HGC timing layer test beam setup.

shower, although most of the results presented below correspond to $6X_0$ of lead. Signals from the HGC timing layer (25 pixels were implemented and read out) and the Photek 240 MCP-PMT are read out and digitized by the CAEN V1742 digitizer; representative signal waveforms for one of the 25 silicon pixels and the Photek 240 are shown in the left and right panel of Figure 10.5, respectively. The silicon signal pulse has a rise time of about 2 ns, and a full pulse width of around 7 ns. This rise time is consistent with a time constant of a silicon sensor coupled to a 50 Ohm amplifier.

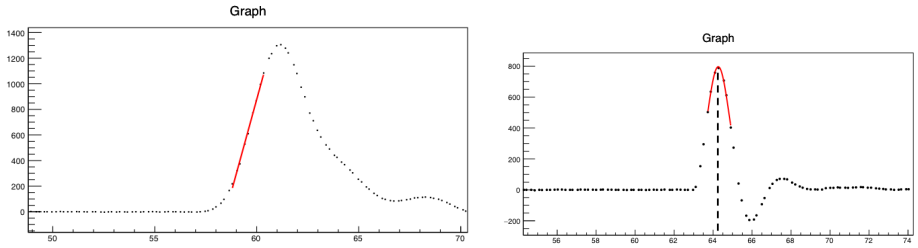

Figure 10.5: Examples of the signal pulse waveform for one the pixels of the HGC timing layer (left) and the Photek MCP-PMT (right) digitized by CAEN V1742 digitizer board. The bias voltage applied to the HGC silicon sensor is −300 V.

The CAEN digitizer is voltage and time calibrated using the procedure described in Ref. [98]. The total collected charge for each signal pulse is computed by integrating

a 10 ns window around the peak of the pulse. The time for the reference Photek 240 MCP-PMT detector is obtained by fitting the peak region of the pulse to a Gaussian function and the mean parameter of the Gaussian is assigned as the timestamp t_0, see the right panel of Figure 10.6. The time for signals from each pixel in the HGC layer is obtained by performing a linear fit to the rising edge of the pulse and the time at which the pulse reaches 45% of the maximum amplitude is assigned as its timestamp t_1, see the left panel of Figure 10.6. The electronic time resolution of the CAEN V1742 digitizer was measured to be ~4 ps and neglected on the timing measurements described below.

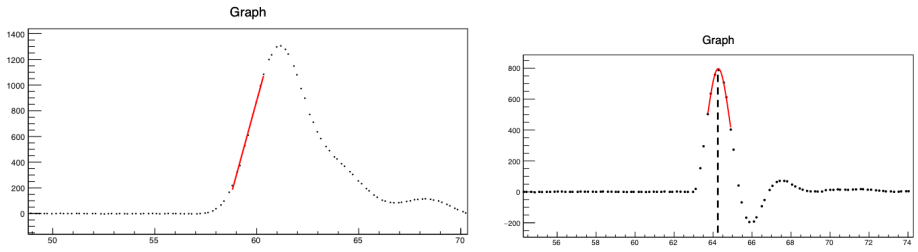

Figure 10.6: Examples of the timestamps extraction for a pulse waveform in one the pixels of the HGC timing layer (left) and the Photek 240 MCP-PMT (right) digitized by CAEN V1742 digitizer board. The timestamp on the HGC pixel is extracted by intersecting the linar fit (solid red line) with the horizonal line corresponding to 45% of the pulse maximum. The timestamp for the Photek 240 is the mean parameter of the Gaussian fit (solid blue line).

Electrons were identified by requiring that the signal amplitude of the Photek 240 MCP-PMT detector, located downstream of the HGC timing layer, exceeds certain thresholds because electromagnetic showers induced by electrons produce significantly larger signals, while pions produce much smaller signals. This procedure has been measured to provide electron purities between 80% and 90% for all beam conditions, see Chapter 9.

Intrinsic HGC TOF resolution

Let's now examine the intrinsic timing capabilities of the HGC layer. The HGC timing layer was positioned just downstream of $6X_0$ of lead and showering electrons were selected by requiring the signal amplitude and integrated charge in the Photek 240 MCP-PMT to be above a certain threshold. Figure 10.7 shows two examples of transeverse shower profile measured by the HGC layer, where the color palette represents the integrated charge in each pixel. As observed in Figure 10.7 most of the activity is concentrated in the central and the 6 neighbouring pixels – these 7 pixel are

more clearly reprensented in the left panel of Figure 10.1 – and therefore the studies in this chapter just include these pixels. It is of note that the central pixel could fluctuate in an event-by-event basis. The TOF for each of the considered pixels in the

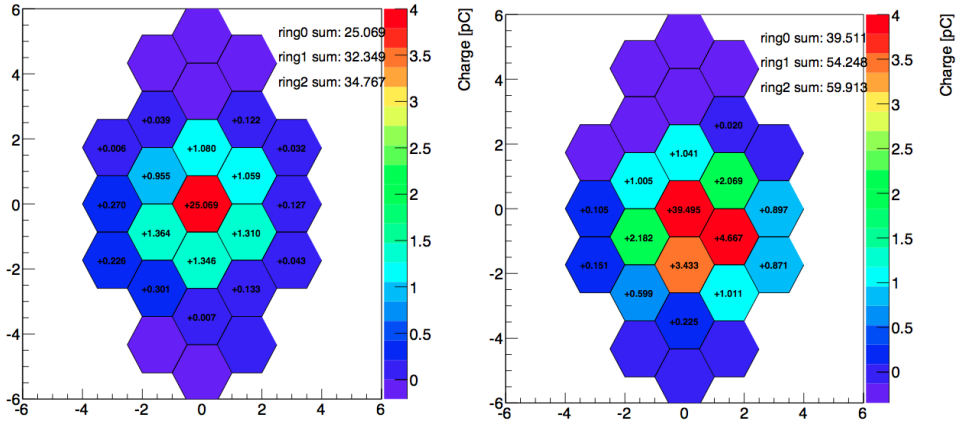

Figure 10.7: Examples of the shower transverse profile sampled by the HGC layer for a 32 GeV (left) and 16 GeV (right) electron beam. There is $6X_0$ of tungsten right upstream of the HGC layer.

HGC layer with respect to the Photek 240 MCP-PMT, i.e. $\Delta t = t_1 - t_0$, is calculated. Subsequently, the information from all the pixels is combined by weighting the individual times with the corresponding charge deposited in the following fashion:

$$\Delta t_{HGC} = \frac{\sum_{i=0}^{6} \text{charge}_i \times \Delta t_i}{\sum_{i=0}^{6} \text{charge}_i}, \tag{10.1}$$

where Δt_{HGC} is the combined HGC layer TOF, charge_i is the charge deposited in the i-th pixel, and Δt_i is the i-th pixel TOF. The TOF distributions for the pixels with highest and second highest charge are shown in the left and right panel of Figure 10.8, respectively. The TOF distributions of the HGC layer (Δt_{HGC}) is shown in the left panel of Figure 10.9, while an alternative method for combining the HGC pixels – using the most probable value (mpv) of the deposited charge distribution in each pixel as the weight, see Eq. 10.1. These weights are constant throughout an entire run. – is shown in the right panel of Figure 10.9. It is of note that the default and the alternative (mpv) algorithms yield very similar results with an outstanding time resolution of about 15 ps for an electron beam of 32 GeV.

Comparing Figure 10.8 (left panel) and Figure 10.9, it is observed that the TOF resolution of the central pixel is already close the final time resolution of the entire

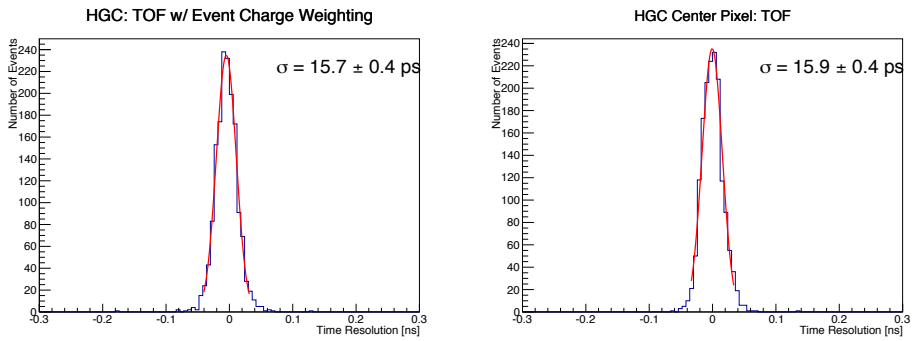

Figure 10.8: TOF distributions for (left) the pixel with the highest and (right) the the pixel with the second highest charge in the HGC layer using a 32 GeV electron beam and $6X_0$ of tungsten. The TOF resolutions are estimated by the standard deviation parameter of the Gaussian fit (red solid curve) to the TOF distribution.

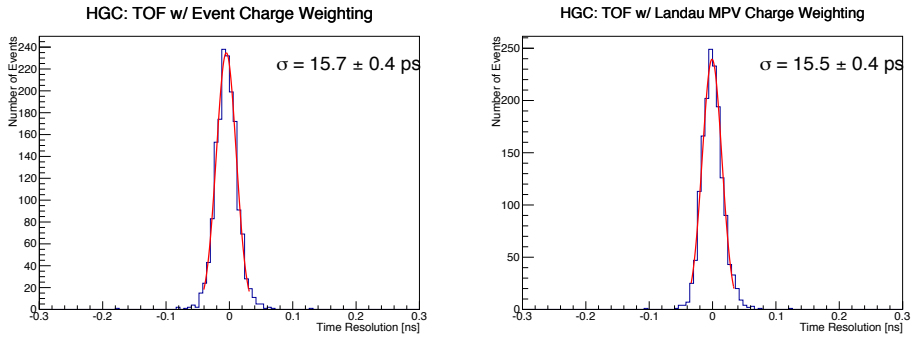

Figure 10.9: TOF distributions of the HGC layer using a 32 GeV electron beam and $6X_0$ of tungsten, where the pixels are combined with (left) the default algorithm and (right) the mpv of the charge distribution as the weight. The TOF resolutions are estimated by the standard deviation parameter of the Gaussian fit (red solid curve) to the TOF distribution .

HGC layer. This suggests that pixels combination does not provide a significant improvement to the overall TOF resolution. Figure 10.10 shows the HGC TOF resolution as a function of the pixels combined at different separations between the tunsten absorber and the HGC layer, where it is observed that the TOF resolution is not significantly improved as a function of the added pixels for any of the separations. Despite the small improvement, it is observed that the larger the distance between the absorber and the HGC layer the larger is the relative improvement in the time resolution as more pixels are added, this is consistent with the fact that showers are more spread for the runs with more separation. Thus, it is convenient to define a quantity related to the transverse shower spread, to achive this we use the ratio of the charge in the central pixel and the total charge in the 7 pixels as proxy to the

transverse showe profile:

$$R_7 = \frac{\text{charge}_0}{\sum_{i=0}^{6} \text{charge}_i}, \tag{10.2}$$

where $charge_i$ is the charge deposited in the i-th pixel, with the zeroth being the central pixel. The R_7 distribution is shown in Figure 10.11.

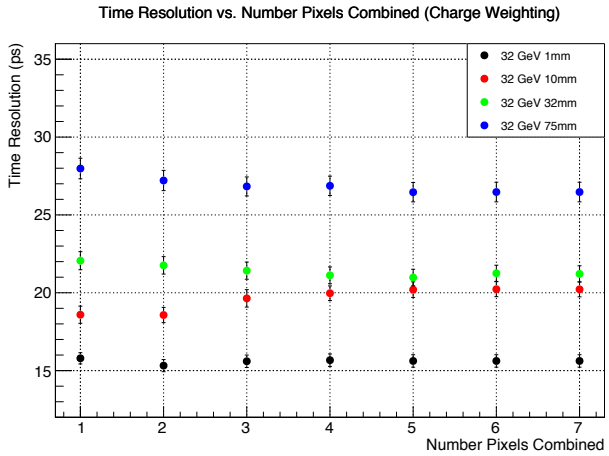

Figure 10.10: HGC layer TOF resolution as a function of the number of pixels combined. The distance between the absorber and the HGC layer was varied to sample the shower at different location.

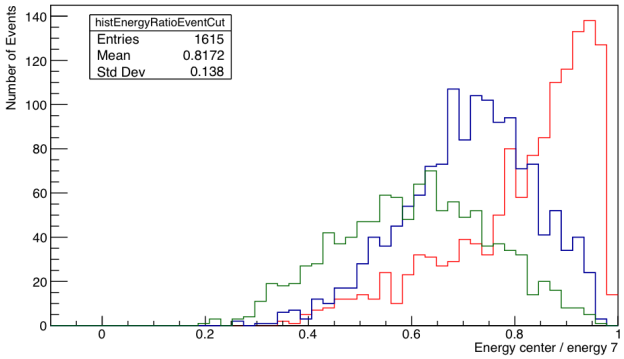

Figure 10.11: R_7 distribution for different separations between the HGC layer and the $6X_0$ of tungsten.

Combining Two Timing Layers

Combining the timing information of multiple HGC layers could improve the final TOF resolution of the calorimeter to em showers. The measurements presented in

this chapter lack of an identical second HGC layer, but as shown in Chapter 8 the Photonics MCP-PMT localted downstream of the HGC layer could be use as an additional timing measurement. To obtain the final TOF measurement (two-layer combination) the HGC layer and the Photonis MCP-PMT are combined with an equal weigh. Figure 10.12 shows the TOF distribution for the Photonis MCP-PMT and the final two-layer combination in the left and right panels, respectively.

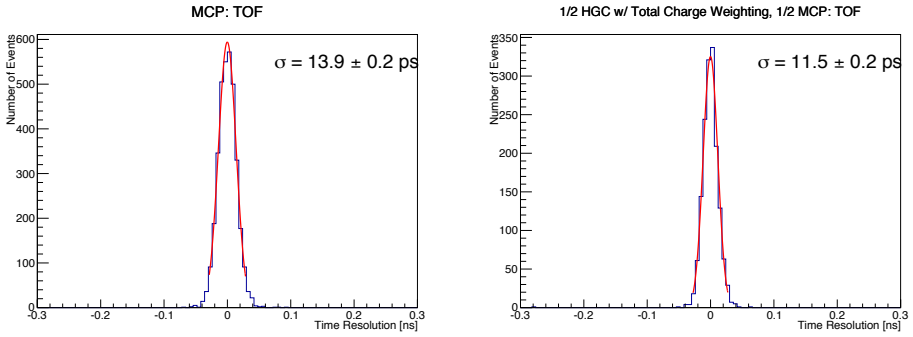

Figure 10.12: TOF distributions for (left) the Photonis MCP-PMT and (right) the final two-layer combination using a 32 GeV electron beam and $6X_0$ of tungsten. The TOF resolutions are estimated by the standard deviation parameter of the Gaussian fit (red solid curve) to the TOF distribution .

Emulation of SKIROC2 Readout

The HGC proposed for the Phase 2 Upgrade of the CMS electromagnetic calorimeter uses a fron-end electronics readout based on the *SKIROC2* chip, which has been preliminary shown to have around 50 ps jitter[45]. In order to simulate the effect of having a *SKIROC2* readout, the studies just presented above are now repeated with all the measured timestamps randomly smeared by 50 ps. Each timestamp – this includes all the HGC layer pixels, the Photonis MCP-PMT, and the reference Photek 240 MCP-PMT. – is smeared by adding a random number drawn from a Gaussian p.d.f with a mean and a width of 0 and 50 ps, respectively.

Figure 10.13 shows the TOF distributions after smearing for the pixels with highest and second highest charge in the left and right panel, respectively. The Δt_{HGC} distribution and the two-layer combination TOF distribution are shown in the left and right panel of Figure 10.14. Here, pixels and layer are all combined with the same weight. The HGC time resolution improves from that of the central pixel only, this could be explain since the dominance of the central pixels has been diluted by the 50 ps Gaussian smearing. The HGC time resolution as a function of the number

of pixels combined is shown in Figure 10.15. It is of note that the final two-layer combination time resolution for a 32 GeV electron beam is around 30 ps and meets the requirements needed to reject pileup at the HL-LHC (30 ps is equivalent to 1 cm resolution in the collision axis).

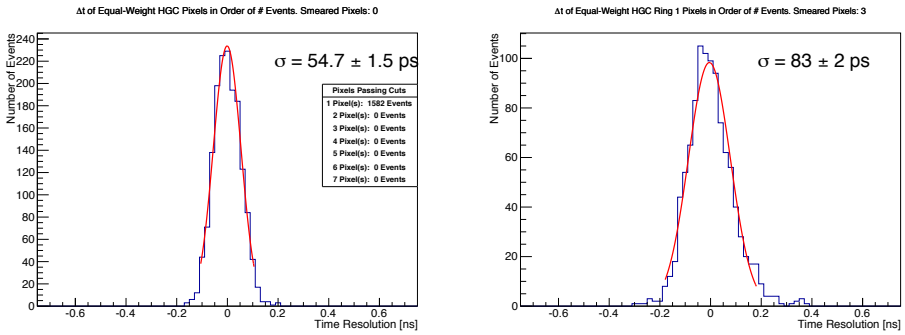

Figure 10.13: TOF distributions after a 50 ps Gaussian smearing for (left) the pixel with the highest and (right) the the pixel with the second highest charge in the HGC layer using a 32 GeV electron beam and $6X_0$ of tungsten. The TOF resolutions are estimated by the standard deviation parameter of the Gaussian fit (red solid curve) to the TOF distribution.

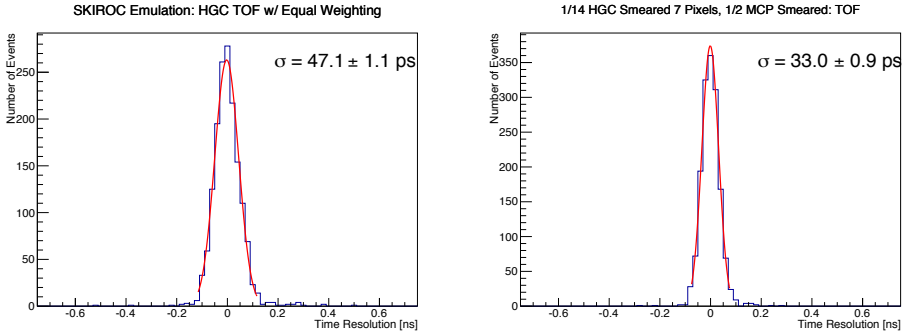

Figure 10.14: TOF distributions after a 50 ps Gaussian smearing for (left) the HGC layer and (right) the final two-layer combination using a 32 GeV electron beam and $6X_0$ of tungsten. The TOF resolutions are estimated by the standard deviation parameter of the Gaussian fit (red solid curve) to the TOF distribution.

10.5 Dicussion and Conclusions

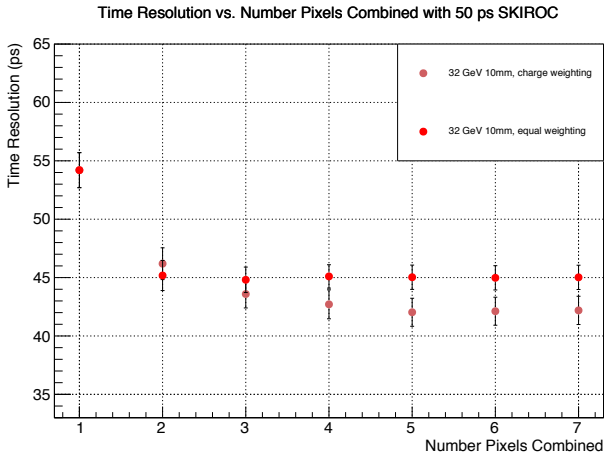

Figure 10.15: HGC layer TOF resolution after a 50 ps Gaussian smearing as a function of the number of pixels combined.